Title

Optimized scintillator YAG:Pr nanoparticles for X-ray inducible photodynamic therapy

Authors

Sapre, Ajay A
Novitskaya, Ekaterina
Vakharia, Ved
et al.

Publication Date

2018-10-01

DOI

10.1016/j.matlet.2018.05.090

Peer reviewed

Materials Letters 228 (2018) 49–52

Contents lists available at ScienceDirect

Materials Letters

journal homepage: www.elsevier.com/locate/mlblue

Optimized scintillator YAG:Pr nanoparticles for X-ray inducible photodynamic therapy

Ajay A. Sapre [a,1], Ekaterina Novitskaya [b,1], Ved Vakharia [b], Alejandro Cota [b], Wolfgang Wrasidlo [c], Stephen M. Hanrahan [d], Stephen Derenzo [d], Milan T. Makale [e,*], Olivia A. Graeve [b,*]

[a] University of California, San Diego, Department of Bioengineering, 9500 Gilman Drive – MC 0412, La Jolla, CA 92093-0412, USA
[b] University of California, San Diego, Department of Mechanical and Aerospace Engineering, 9500 Gilman Drive – MC 0411, La Jolla, CA 92093-0411, USA
[c] University of California, San Diego, Department of Neurosciences, 9500 Gilman Drive – MC 0662, La Jolla, CA 92093-0662, USA
[d] Lawrence Berkeley National Laboratory, Molecular Biophysics and Integrated Bioimaging Division, Cellular and Tissue Imaging Department, 1 Cyclotron Road, M/S 55-121, Berkeley, CA 94720, USA
[e] University of California, San Diego, Department of Radiation Medicine and Applied Sciences, 3855 Health Sciences Drive #0819, La Jolla, CA 92093-0819, USA

ARTICLE INFO

Article history:
Received 27 December 2017
Received in revised form 4 May 2018
Accepted 19 May 2018
Available online 20 May 2018

Keywords:
YAG
Praseodymium
X-ray inducible photodynamic therapy
Nanoparticles
Scintillator

ABSTRACT

We describe a sol-gel synthetic method for the production of praseodymium-doped yttrium aluminum garnet (YAG) nanoparticles suitable for X-ray inducible photodynamic therapy (X-PDT). Our sol-gel based approach was optimized by varying temperature and time of calcination, resulting in nanoparticles that were smooth, spherical, and 50–200 nm in crystallite size. The powders were uniformly coated with a thin (10 nm) layer of silica to facilitate surface conjugation with functional moieties. Measurements of photon flux revealed that coated and uncoated powders emitted a similar photon emission spectrum in response to 50 keVp X-rays. We also determined that the presence of silica did not significantly reduce flux and the emission peak had a maximum at approximately 320 nm. Thus, these YAG:Pr powders are suitable candidates for future *in vivo* X-PDT studies.

1. Introduction

Cancer is a leading cause of death and virtually all front-line chemotherapy drugs and radiation therapies are nonspecific, leading to systemic toxicity and acquired resistance. Hence, radiation oncologists have long proposed the concept of a prodrug that is activated by radiation only at a tumor site. Such a prodrug, administered in a nontoxic form, would circulate through the blood and be taken up by the tumor, where it would be activated with a radiation beam aimed only at the tumor [1]. This strategy allows for delivery of high doses of prodrug that is activated only at the site of interest, thereby reducing off target side effects. The development of radiation prodrugs has been stymied because dissolved oxygen, which is ubiquitous in mammalian tissues, quenches chemical species needed to trigger prodrug activation [2–5]. A recent approach, X-ray inducible photodynamic therapy (X-PDT) [6], offers a potential solution based on radiation scintillator materials that emit light in response to ionizing radiation such as X-rays [7]. The X-PDT concept makes use of an inactive light sensitive prodrug or a photosensitizer, which produces singlet oxygen upon exposure to emitted light, coupled to a scintillator nanoparticle [8]. The nanoparticles, when injected into the blood, are expected to mainly distribute to tumor tissue, as well as the liver and spleen from which they will eventually clear [9]. After distribution, ionizing radiation directed only at the tumor triggers scintillator light emission to locally induce prodrug conversion or photosensitizer activation and, in fact, X-PDT has elicited tumor shrinkage in animal tumor models [10].

A variety of scintillator materials have been proposed for X-PDT, including $LaF_3:Ce^{3+}$, $LuF_3:Ce^{3+}$, $CaF_2:Mn^{2+}$, $CaF_2:Eu^{2+}$, BaFBr:Eu^{2+}, and semiconductors such as ZnO, ZnS and TiO_2 [11]. Rare-earth doped yttrium aluminum garnet [$(Y_{1-x}RE_x)_3Al_5O_{12}$ (with $x < 0.01$)] is one material that, to our knowledge, has not been tested extensively for X-PDT [12,13]. When this material is doped with praseodymium [$(Y_{1-x}Pr_x)_3Al_5O_{12}$ or YAG:Pr] it offers several distinct advantages including high quantum efficiency, tunability of emitted light wavelength, and the very low biological toxicity of yttrium, praseodymium, and aluminum [14–16].

In therapeutic applications, scintillator materials need to have certain design characteristics in order to be biologically compatible

* Corresponding authors.
E-mail addresses: mmakale@ucsd.edu (M.T. Makale), ograeve@ucsd.edu (O.A. Graeve).
URL: http://graeve.ucsd.edu (O.A. Graeve).
[1] These authors contributed equally to this work.

https://doi.org/10.1016/j.matlet.2018.05.090
0167-577X/

and be able to effectively accumulate in tumor tissue. These include proper crystallite size of the powders, to take advantage of tumor accumulation *via* the enhanced permeability and retention (EPR) effect, and smooth spherical particles to minimize blood vessel wall damage and to allow uniform loading of the desired payload [17,18]. For passive targeting *via* EPR, optimal crystallite size is generally agreed to be between 10 and 200 nm [19]. Crystallite sizes that are too large will be rapidly removed by the reticuloendothelial and hepatic systems, while crystals smaller than 5 nm will be quickly cleared by the kidneys [20]. Thus, the preparation of spherical, smooth, and appropriately sized scintillator powders is critical for their use in X-PDT. However, the majority of reported YAG powders, have not been prepared for biological applications and are not appropriately configured for *in vivo* use.

Moszynski et al. [21] was among the first to synthesize rare earth doped YAG powders, but did not characterize their size and shape. Zhou et al. [12] produced yttrium-based particles, which were too small for most biomedical applications involving intravenous administration. Additionally, their TEM images appeared to show irregularly-shaped particles. Other compositions have also possessed disqualifying properties. For example, Chen et al. [6] developed $SrAl_2O_4:Eu^{2+}$ loaded with a photosensitizer, namely merocyanine 540 (MC540) that yielded cytotoxic oxygen species when exposed to light. These irregularly-shaped particles were smoothed with a comparatively thick silica coating, but were unstable and ultimately too large (mean diameter = 407.4 ± 152.5 nm) for relevant preclinical development in animal models and especially for clinical use in patients. In this context, and given the compelling attributes of YAG:Pr scintillator materials, we were motivated to develop a sol-gel synthetic methodology for the preparation of YAG nanocrystals that could be evenly and thinly coated. Sol-gel powder fabrication techniques have been reported to offer superior shape and size control for the preparation of YAG [22–27]. The process can be effective with appropriate selection of precursors and calcination temperature and time.

In this report, we present an optimized sol-gel based scheme for the production of silica-coated YAG:Pr scintillator nanoparticles displaying the desired physical shape and size characteristics for X-PDT applications. The specific criteria used to assess the YAG:Pr scintillator included an emitted light wavelength between 300 and 400 nm, spherical or near-spherical crystal shape, a uniform and smooth surface, and crystallite diameters between 50 and 200 nm.

2. Experimental procedures

$(Y_{1-x}Pr_x)_3Al_5O_{12}$ (with $x = 0.01$) nanocrystals were prepared using a so-gel synthesis technique using praseodymium (III) nitrate hexahydrate [$Pr(NO_3)_3{\cdot}6H_2O$, 99.99%, Alfa Aesar, Ward Hill, MA] as a source of praseodymium, nanosized (50 nm) Al_2O_3 [Sky-Spring Nanomaterials, Inc., Houston, TX] as a source of aluminum, and yttrium (III) 2,4-pentanedionate hydrate [$Y(C_5H_7O_2)_3$, 99.9%, Alfa Aesar, Ward Hill, MA] as a source of yttrium. A mixture of 0.0183 g of $Pr(NO_3)_3{\cdot}6H_2O$, 2.1451 g of Al_2O_3, and 4.8591 g of $Y(C_5H_7O_2)_3$ were dissolved in 75 mL of methanol. The solution was stirred at 400 rpm for approximately 48 h (until the entire liquid methanol had evaporated). The mostly dry, whitish-yellow product was then removed from the beaker and crushed with a mortar and pestle in preparation for pre-calcination. The crushed powders were heated in a box furnace (SenroTech) for 1 h at 500 °C (pre-calcination step) to remove carbon impurities. Powders were calcined at different temperatures for varying times: 2 h at 1000 °C, 2 h at 1100 °C, 2 h at 1200 °C, 1 h at 1350 °C, and 1 h at 1400 °C. The calcination time was chosen to be 1–2 h to prevent undesired nanoparticle growth. Additionally, the calcination procedure for the samples calcined at 1000 °C, 1100 °C, and 1200 °C consisted of 3 h ramp up and 3 h ramp down stages of the heating and cooling processes. The samples calcined at 1350 °C and 1400 °C were placed in the furnace preheated to the maximum calcination temperature, that is, there was no ramp up and ramp down stages. For application of the silica coating, the YAG:Pr powders were diluted in ethanol at 0.1 mg/mL. Tetramethyl orthosilicate (TMOS) [MW = 152.22, purity = 98%, vapor density = 5.25 (vs air), Sigma-Aldrich] was hydrolyzed in 1 mM HCl at 14% by volume to form silicic acid. Typically, 3.75 μL TMOS and 25 μL 1 mM HCl for 1 min was used. To coat the powders, a mixture of 0.05% (v/v) silicic acid was prepared with the solution containing 0.01 mg/mL of particles and vortexed overnight at room temperature. The unreacted silicic acid was removed by centrifuging the coated particles and washing with ethanol three times. To reduce aggregation, samples were probe sonicated using a QSonica Q125 (QSonica, Newton, CT) at 30% amplitude for 2 min.

Phases of the powders were characterized by X-ray diffraction (XRD) on a D2 Phaser (Bruker AXS, Madison, WI) using a step size of 0.02° 2θ and a count time of 1 s by scanning from 15 to 85° 2θ. Particle morphology of uncoated and coated powders were observed using a G2 Sphera (FEI Company, Hillsboro, OR) transmission electron microscope (TEM) using a 200 keV accelerating voltage. For TEM sample preparation, powders were dissolved in acetone (1 mg/mL), ultrasonicated for 15 min, and stirred for 15 min. Subsequently, the solution containing dispersed powder was dropped onto a thin carbon-coated copper TEM grid. The luminescence of the samples was measured by placing 265 mg of YAG:Pr powder in glass cuvettes of approximately 500 μL volume. The samples were excited by a continuous unfiltered X-ray beam from a Nonius FR591 water-cooled rotating copper-anode X-ray generator (Bruker AXS Inc., Madison, WI) set at 50 kV and 60 mA. The emission spectra were measured with a SpectraPro-2150i spectrometer (Acton Research Corp., Acton, MA) coupled to a PIX-IS:100B charge-coupled detector (CCD) (Princeton Instruments, Inc., Trenton, NJ). The spectrometer has a motorized order-sorting filter wheel, a motorized slit, and two diffraction gratings (blazed for 300 and 500 nm) mounted on a turret. The order-sorting filters eliminated all second or higher order peaks. Three exposures were used to cover the 200–1000 nm range.

3. Results and discussion

The X-ray diffraction patterns for the powders at different temperatures and times of calcination are illustrated in Fig. 1. Peaks correspond to YAM ($Y_4Al_2O_9$), YAP ($YAlO_3$), and YAG ($Y_3A_5O_{12}$) phases, with variations in phase formation correlated to the time and temperature of calcination. Additionally, aluminum oxide was quite prominent at the lower calcination temperatures (Fig. 1(a) and (b)), while it became significantly smaller at 1200 °C (Fig. 1(c)), a qualitative assessment based on the height of the peaks. This phase is almost completely eliminated at the higher temperatures of 1350 °C and 1400 °C (Fig. 1(d) and (e)). There were no YAG peaks at temperatures less than 1100 °C and, instead, prominent YAM and YAP peaks were observable (Fig. 1(a) and (b)). This is in contrast to other sol-gel based studies, which report the presence of YAG at 800 °C [22], 900 °C [23], 950 °C [24], and 1000 °C [25]. These differences can be attributed to relatively minor variations in preparative methods and/or differences in precursors. For example, Zhou et al. [22], prepared YAG powders through a polymer-assisted sol-gel method with citric acid, acrylamide (AAM), and N,N′-methylenebisacrylamide (MBAAm) introduced into the solution before it was dried into a powder. Marin et al. [25] made use of heating to 100 °C with stirring, whereas Li et al. [23] and Ruan et al. [24] used stabilizing acids with heated

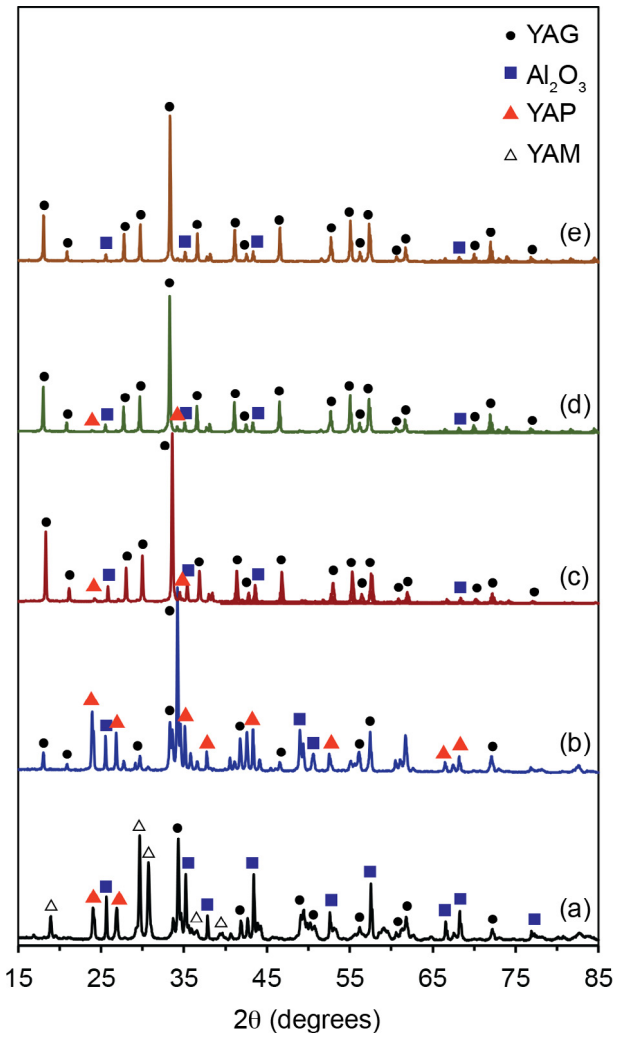

Fig. 1. X-ray diffraction patterns of the powders calcined at (a) 1000 °C for 2 h, (b) 1100 °C for 2 h, (c) 1200 °C for 2 h, (d) 1350 °C for 1 h, and (e) 1400 °C for 1 h.

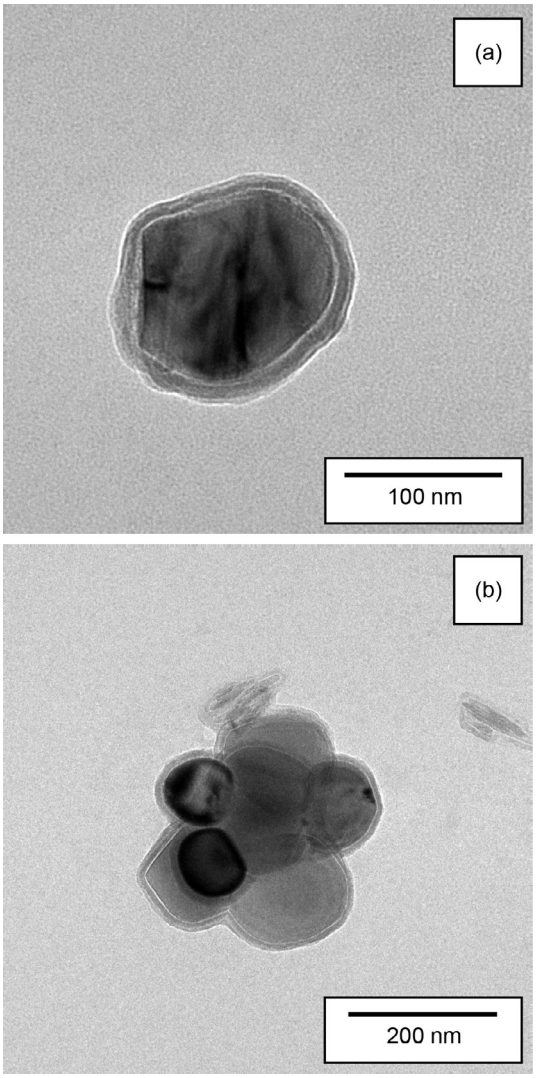

Fig. 2. TEM images showing thin silica coating of (a) unagglomerated YAG:Pr particles and (b) slightly agglomerated YAG:Pr particles, clearly visible as a light gray encapsulating layer.

stirring. Our study did not incorporate acid-based stabilization and heat was not applied during the stirring step of the synthesis process.

As calcination temperature increased from 1100 °C to 1200 °C, the powder diffraction pattern began to match that of the YAG phase (compare Fig. 1(b) and Fig. 1(c)). Furthermore, the YAM phase disappeared at 1100 °C, and the YAP phase became less evident between 1000 °C and 1100 °C; both of these phases almost completely vanished by 1200 °C (Fig. 1(c)). These results agree with Ogi et al. [26,27] who reported the preparation of YAG:Ce by sol-gel synthesis and calcination at 1400 °C, but did not comment on the status of YAM or YAP phases at lower calcination temperatures. Our results also corroborate with those of Li et al. [23] and Ruan et al. [24] who reported the sol-gel synthesis of YAG powders using co-precipitated precursors different from ours. In addition, a study by Simoneko et al. [28] showed YAG and YAP phases in a powder prepared by heating a xerogel in air flow at a temperature of 990 °C, while only YAG was present in powder calcined at 1200 °C.

Empirically, the 1400 °C calcination treatment results in optimum powders because of a balance between the formation of the desired YAG phase, the shortened calcination time (1 h vs. 2 h) that minimizes agglomeration, and diffusion processes during nanoparticle growth that may help in eliminating jagged edges. Thus, the powders calcined at 1400 °C were used for subsequent coating with silica to provide a means of conjugating functional molecules, such as targeting ligands to the particle surfaces. Fig. 2(a) and (b) illustrates the YAG:Pr powders coated with silica, which formed a uniform and thin (10 nm) layer. Silica was chosen as it is non-toxic, FDA approved, and amenable to a variety of surface chemistries through silanol groups [29].

The particle photon emission spectra for the uncoated and silica coated YAG:Pr particles, in response to 50 keVp X-rays, is provided in Fig. 3. The silica coating reduced the measured peak photon flux by about 25%, as it served as a barrier to light transmission. Nonetheless, as shown by Fig. 3, the absolute photon flux was still robust and the peak wavelength was unaffected, remaining at 320 nm. Hence, we conclude that the silica coated particles exhibit an emission spectrum that is operationally similar compared to the uncoated particles. This suggests that coating YAG:Pr particles with silica may be a feasible approach for introducing functional groups to the particle surfaces and will not adversely compromise nanoscintillator photon emission.

In summary, the regular surface of the YAG:Pr nanoparticles allowed the efficient and complete coating with a 10 nm layer of silica for further surface functionalization. Some of the agglomeration was resolvable by mild ultrasonication and the coated

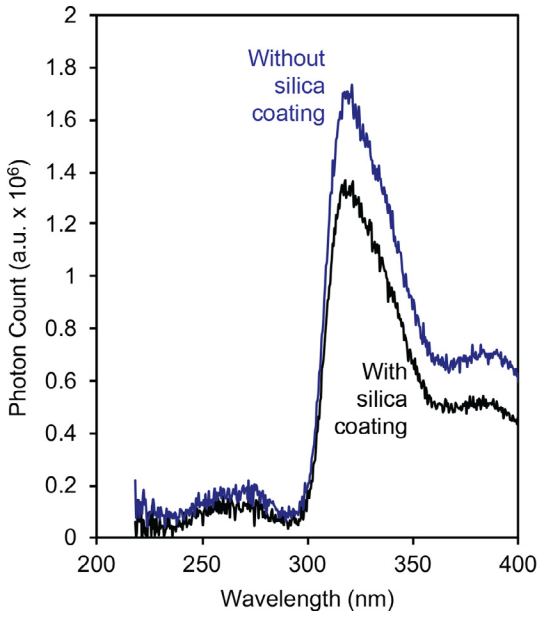

Fig. 3. Particle photon emission spectra in response to 50 keVp X-rays for uncoated and silica coated YAG:Pr particles.

particles exhibited a minimal reduction in photon flux during radiation exposure due to the coating. Given these attributes, we believe that our YAG:Pr powders are well-suited for further development in an X-PDT treatment system.

4. Conclusions

We describe the preparation of smooth, spherical scintillator nanoparticles of $(Y_{1-x}Pr_x)_3Al_5O_{12}$ (YAG:Pr) with $x = 0.01$. The optimized sol-gel process was straightforward and included the key step of calcination at 1400 °C for 1 h. Corresponding phases and crystallite sizes of the powders were characterized by X-ray diffraction, together with transmission electron microscopy (TEM), while particle sizes and morphologies were evaluated by TEM. The overall diameter of the nanocrystals was found to be less than 200 nm. Moreover, a uniform coating of the crystals with a thin, functionalizing silica layer proved to be feasible. Coated and uncoated powders exhibited a similar photon emission profile, and photon flux with coated particles remained robust. Collectively, these observations suggest that sol-gel prepared YAG:Pr nanoparticles may be suitable for *in vivo* preclinical and clinical X-PDT studies.

5. Acknowledgements

This research was supported in part by National Institutes of Health grant 1R21CA187528-01 to M. Makale and National Science Foundation grant 1334160 to O.A. Graeve. We acknowledge the use of the UCSD Cryo-Electron Microscopy Facility, which is supported by National Institutes of Health grants to T.S. Baker and a gift from the Agouron Institute to UC San Diego.

References

[1] W.A. Denny, Tumor-activated prodrugs–a new approach to cancer therapy, Cancer Invest. 22 (2004) 604–619.
[2] K. Tanabe, Y. Mimasu, A. Eto, Y. Tachi, S. Sakakibara, M. Mori, H. Hatta, S. Nishimoto, One-electron reduction characteristics of N(3)-substituted 5-fluorodeoxyuridines synthesized as radiation-activated prodrugs, Bioorg. Med. Chem. 11 (2003) 4551–4556.
[3] L.P. Candeias, J. Wildeman, G. Hadziioannou, J.M. Warman, Pulse radiolysis – optical absorbtion studies on the triplet states of p-phenylenevinylene oligomers in solution, J. Phys. Chem. 104 (2000) 8366–8371.
[4] N. Fujisaki, S. Shida, Y. Hatano, K. Tanno, The Radiolysis of liquid n-butane, J. Phys. Chem. 76 (1971) 2854–2860.
[5] H.D. Burrows, M. da G.. da Miguel, A.P. Monkman, L.E. Horsburgh, Pulse radiolysis studies on charge carrying polymers, J. Chem. Phys. 112 (2000) 3082–3089.
[6] H. Chen, G.D. Wang, Y.-J. Chuang, Z. Zhen, X. Chen, P. Biddinger, Z. Hao, F. Liu, B. Shen, Z. Pan, J. Xie, Nanoscintillator-mediated X-ray inducible photodynamic therapy for in vivo cancer treatment, Nano Let. 15 (2015) 2249–2256.
[7] C. Greskovich, S. Duclos, Ceramic scintillators, Annu. Rev. Mater. Sci. 27 (1997) 69–88.
[8] G.D. Wang, H.T. Nguyen, H. Chen, P.B. Cox, L. Wang, K. Nagata, Z. Hao, A. Wang, Z. Li, J. Xie, X-ray induced photodynamic therapy: a combination of radiotherapy and photodynamic therapy, Theranostics. 6 (2016) 2295–2305.
[9] M. Yu, J. Zheng, Clearance pathways and tumor targeting of imaging nanoparticles, ACS Nano 9 (2015) 6655–6674.
[10] A.Z. Wang, R. Langer, O.C. Farokhzad, Nanoparticle delivery of cancer drugs, Annu. Rev. Med. 63 (2012) 185–198.
[11] N.Y. Morgan, G. Karamer-Marek, P.D. Smith, K. Camphausen, J. Capala, Nanoscintillator conjugates as photodynamic therapy based radiosensitizers: Calculation of required physical parameters, Radiat. Res. 171 (2009) 236–244.
[12] S. Zhou, Z. Fu, J. Zhang, S. Zhang, Spectral properties of rare-earth ions in nanocrystalline YAG: Re (Re = C^{e3}+, P^{r3}+, T^{b3}+), J. Lumin. 118 (2006) 179–185.
[13] J. Jung, G. Hirata, G. Gundiah, S. Derenzo, W. Wrasidlo, S. Kesari, M.T. Makale, J. McKittrick, Identification and development of nanoscintillators for biotechnology applications, J. Lumin. 118 (2014) 569–577.
[14] U. Vitolo, G. Barosi, S. Fanti, A.M. Gianni, M. Martelli, M. Petrini, P.L. Zinzani, S. Tura, Consensus conference on the use of 90-yttrium-ibritumomab tiuxetan therapy in clinical practice. A project of the Italian society of hematology, Am. J. Hematol. 85 (2010) 147–155.
[15] K.T. Rim, K.H. Koo, J.S. Park, Toxicological evaluations of rare earths and their health impacts to workers: a literature review, Saf. Health Work 4 (2013) 12–26.
[16] L. Tomljenovic, Aluminum and Alzheimer's disease: after a century of controversy, is there a plausible link?, J Alzheimers Dis. 23 (2011) 567–598.
[17] A. Albanese, P.S. Tang, W.C.W. Chang, The effect of nanoparticle size, shape and surface chemistry on biological systems, Annu. Rev. Biomed. Eng. 14 (2012) 1–16.
[18] J. Fang, H. Nakamura, H. Maeda, The EPR effect: unique features of tumor blood vessels for drug delivery, factors involved, and limitations and augmentation of the effect, Adv. Drug Delivery. Rev. 63 (2010) 136–151.
[19] H. Kobayashi, R. Watanabe, P.L. Choyke, Improving conventional enhanced permeability and retention (EPR) effects; what is the appropriate target?, Theranostics 4 (2014) 81–89.
[20] H.S. Choi, W. Liu, P. Misra, E. Tanaka, J.P. Zimmer, B.I. Ipe, M.G. Bawendi, J.V. Frangioni, Renal clearance of nanoparticles, Nat. Biotechnol. 25 (2007) 1165–1170.
[21] M. Moszynski, T. Ludziejewski, D. Wolski, W. Klamra, L.O. Norlin, Properties of the YAG: Ce scintillator, Nucl. Instr. Meth Phys. Res. A 345 (1994) 461–467.
[22] X. Zhou, K. Zhou, Y. Li, Z. Wang, Q. Feng, Luminescent properties and energy transfer of $Y_3Al_5O_{12}$:Ce^{3+}, Ln^{3+}, (Ln = Tb, Pr) prepared by polymer-assisted sol-gel method, J. Lumin. 132 (2012) 3004–3009.
[23] J.-G. Li, T. Ikegami, J.-H. Lee, T. Mori, Y. Yajima, Co-precipitation synthesis and sintering of yttrium aluminum garnet (YAG) powders: the effect of precipitant, J. Eur. Ceram. Soc. 20 (2000) 2395–2405.
[24] S.-K. Ruan, J.-G. Zhou, A.-M. Zhong, J.-F. Duan, X.-B. Yang, M.-Z. Su, Synthesis of $Y_3Al_5O_{12}$:Eu^{3+} phosphor by sol-gel method and its luminescence behavior, J. Alloy. Compd. 275–277 (1998) 72–75.
[25] R. Marin, G. Sponchia, P. Riello, R. Sulcis, F. Enrichi, Photoluminescence properties of YAG:Ce^{3+}, P^{r3}+ phosphors synthesized via the Pechini method for white LEDs, J. Nanopart. Res. 14 (2012) 866–914.
[26] T. Ogi, A. Nandiyanto, W.-N. Wang, F. Iskandar, K. Okuyama, Direct synthesis of spherical YAG: Ce phosphor from precursor solution containing polymer and urea, Chem. Eng. J. 210 (2012) 461–466.
[27] T. Ogi, A. Nandiyanto, K. Okino, F. Iskandar, W.-N. Wang, E. Tanabe, K. Okuyama, Towards better phosphor design: Effect of SiO_2 nanoparticles on photoluminescence enhancement of YAG:Ce, ECS J. Solid State Sci. Technol. 2 (2013) R91–R95.
[28] E. Simoneko, N. Simoneko, V. Sevastyanov, N.T. Kuznetsov, Synthesis of ultrafine yttrium aluminum garnet using sol-gel technology, Russ. J. Inorg. Chem. 57 (2012) 1521–1528.
[29] A. Liberman, N. Mendez, W.C. Trogler, A.C. Kummel, Synthesis and surface functionalization of silica nanoparticles for nanomedicine, Surf. Sci. Rep. 69 (2014) 132–158.